IEEE Access
Multidisciplinary | Rapid Review | Open Access Journal

Received August 18, 2019, accepted September 6, 2019, date of publication September 10, 2019,
date of current version September 24, 2020.

Digital Object Identifier 10.1109/ACCESS.2019.2940627

An Improved Empirical Wavelet Transform and Refined Composite Multiscale Dispersion Entropy-Based Fault Diagnosis Method for Rolling Bearing

JINDE ZHENG[1,2], SIQI HUANG[1], HAIYANG PAN[1], AND KUOSHENG JIANG[2]
[1]School of Mechanical Engineering, Anhui University of Technology, Ma'anshan 243032, China
[2]Anhui Key Laboratory of Mine Intelligent Equipment and Technology, Anhui University of Science and Technology, Huainan 232001, China

Corresponding author: Haiyang Pan (pansea@sina.cn)

This work was supported in part by the National Key Research and Development Program of China under Grant 2017YFC0805100, in part by the National Natural Science Foundation of China under Grant 51505002, in part by the University Natural Science Key Project of Anhui Province under Grant KJ2019A053 and Grant KJ2019A092, and in part by the Anhui Key Laboratory of Mine Intelligent Equipment and Technology, Anhui University of Science and Technology, under Grant 201902005.

ABSTRACT The vibration signals collected by the sensor often have non-stationary and non-linear characteristics owing to the complexity of working environment of rolling bearing, so it is difficult to obtain useful and stable vibration information for diagnosis. Empirical Wavelet Transform (EWT) can effectively decompose non-stationary and nonlinear signals, but it is not suitable for signal analysis of bearing with a complicated spectrum. In this paper, an improved EWT (IEWT) method is proposed by developing a new segmentation approach. Meanwhile, the IEWT is compared with empirical mode decomposition (EMD) and EWT to verify the superiority of IEWT in decomposition accuracy. By combining with the refined composite multiscale dispersion entropy (RCMDE), which is a powerful nonlinear tool for irregularity measurement of vibration signals, a new diagnosis method based on IEWT, RCMDE, multi-cluster feature selection and support vector machine is proposed. Then the method is applied to analysis of bearing in this paper and the results show that the new method has higher identifying rate and better performance than that of the methods of RCMDE combining with EMD or EWT. Also, the superiority of RCMDE to dispersion entropy and multiscale dispersion entropy is investigated, together with the superiority of MCFS for feature selection.

INDEX TERMS Fault diagnosis, improved empirical wavelet transform, refined composite multiscale dispersion entropy, feature extraction, rolling bearing.

I. INTRODUCTION

Rolling bearing is an important component of rotating machines and its operating state affects the normal operation of the equipment. Therefore, diagnosing the failure of rolling bearings used in various types of machines is one of the key contents of current research. In the actual working environment, bearing vibration signals are generally affected by external disturbances and thus extracting the hidden fault characteristic information from vibration signals is an important step for diagnosis.

In recent years, the entropy-based complexity feature extraction methods have been continuously applied to mechanical condition monitoring and fault diagnosis areas. Dispersion entropy (DE) [1] is an algorithm for measuring the irregularity and complexity of vibration signals. To overcome the limitations of single-scale analysis, the dispersion entropy is expanded to multiscale framework, i.e. multiscale Dispersion Entropy (MDE) is proposed. However, the MDE will cause the deviation of entropy value obtained in multiscale process [2]. Therefore, by improving the process of coarse graining process in MDE, the Refined Composite Multiscale Dispersion Entropy (RCMDE) [3] is proposed and used in biomedical field [4]–[6]. Generally, the local characteristics of time series cannot be reflected by the coarse-grained of original signal, which only reflects the overall characteristics of time series, and thus the extracted feature information is not completed. Therefore, in this paper, the signal decomposition method is used to separate the time series into several mono-components, then the multiscale entropy value of each mono-component is calculated so that the extracted features contain much more rich fault information.

In 1998, Empirical Mode Decomposition (EMD) first appeared in reference [7], which is proposed by Huang et al,

The associate editor coordinating the review of this manuscript and approving it for publication was Zhixiong Peter Li.

This work is licensed under a Creative Commons Attribution 4.0 License. For more information, see https://creativecommons.org/licenses/by/4.0/

it can effectively decompose the collected original vibration signals into several intrinsic mode functions distributed from high frequency to low frequency. EMD is a data-driven signal decomposition method without choice of base functions and has been affirmed and studied by many scholars [8]–[11]. However, EMD has problems such as endpoint effects and modal mixing [12]–[14]. In 2013, the Empirical Wavelet Transform (EWT) was proposed by Gilles [15], which is different from EMD. EWT is an effective vibration signal decomposition method based on the wavelet transform and its core idea is to establish a suitable filter bank with adaptive bandwidth by adaptively dividing the Fourier spectrum of raw signal. Thus, the raw data can be decomposed into a plurality of amplitude-modulation frequency-modulation (AM-FM) modals with supported Fourier spectrum. Then the Hilbert spectrum of the decomposed AM-FM mode can be obtained, so that a series of meaning instantaneous frequency is obtained [16]. EWT has been widely used in biomedical science [17], [18], seismic analysis [19], mechanical engineering [20]–[22] and other fields. However, the decomposition result of EWT depends on the segmentation of Fourier spectrum, which directly cause different decomposing results for different spectrum segmentation. The spectral segmentation method suitable for a certain field often cannot achieve the expected effect in other fields, so the Fourier spectrum segmentation method is an important factor in the suitability of EWT.

In this paper, to overcome the deficiencies of the maximal midpoint position segmentation method in the original EWT, combined with the vibration signals characteristics of rolling bearings, an improved empirical wavelet transform (IEWT) is proposed based on spectral maxima envelope. Based on that, a new method based on IEWT, RCMDE, multi-cluster feature selection and support vector machine is proposed, and is used in bearing diagnosis. That is, first, the raw signal is decomposed using the IEWT, with several mono-components obtained. Second, the RCMDE of each mono-component is calculated to extract the fault features. Third, the Multi-Cluster Feature Selection (MCFS) [23] is used as a supervised dimensionality reduction of the feature data to eliminate the redundant features extracted by RCMDE from vibration signals and select several sensitive fault features as the sample of classification. Finally, the Support Vector Machine (SVM) [24] can output an optimized separation hyperplane when given some labelled training samples, and is applied to classify the extracted sensitive features to realize the intelligent diagnosis of rolling bearing faults. The proposed fault diagnosis method is compared with the methods of RCMDE combining with EMD or EWT. And the superiority of RCMDE to DE and MDE is investigated, together with the superiority of MCFS in selecting sensitive feature. It can be observed from the results that the new diagnosis method can effectively distinguish the fault type and has a high identification rate than other methods of comparison mentioned above.

The rest of this article is as follows. The EWT and IEWT are introduced in section II and these methods are applied to the simulated signals analysis. The RCMDE algorithm is introduced in section III. The fault diagnostic procedure is given in section IV. In Section V the newly proposed diagnosis method is used in the actual data collected and comparing it with other existing methods. Section VI gives the discussions and conclusions.

II. IMPROVED EMPIRICAL WAVELET TRANSFORM

A. EMPIRICAL WAVELET TRANSFORM METHOD

EWT is a recently proposed adaptive signal decomposition method based on the traditional wavelet transform and it mainly includes two parts, i.e. 1) adaptively looking for segmentation boundaries in Fourier spectrum and 2) construction of wavelet filter bank.

Firstly, the spectrum of the signal $y(t)$ is normalized to $\omega \in [0, \pi]$, assuming ω consists of N continuous intervals $\Lambda_n = [\omega_{n-1}, \omega_n], n = 1, 2, \cdots, N$, where 0 and π are fixed boundaries, the first boundary is $\omega_0 = 0$ and the last boundary is $\omega_N = \pi$. Define a transition section of width $2\tau_n$, which centered on the midpoint ω_n of the two closest maxima in the Fourier spectrum. The empirical scaling function $\widehat{\varphi}_n(\omega)$ and the wavelet function $\widehat{\psi}_n(\omega)$ are represented by Eqs. (1) and (2), respectively:

$$\widehat{\varphi}_n(\omega) = \begin{cases} 1, & |\omega| \le \omega_n - \tau_n \\ \cos\{\frac{\pi}{2}\beta[\frac{1}{2\tau_n}(|\omega| - \omega_n + \tau_n)]\}, & \omega_n - \tau_n \le |\omega| \le \omega_n + \tau_n \\ 0, & otherwise \end{cases} \tag{1}$$

$$\widehat{\psi}_n(\omega) = \begin{cases} 1, & \omega_n + \tau_n \le |\omega| \le \omega_{n+1} - \tau_{n+1} \\ \cos\{\frac{\pi}{2}\beta[\frac{1}{2\tau_{n+1}}(|\omega| - \omega_{n+1} + \tau_{n+1})]\}, & \omega_{n+1} - \tau_{n+1} \le |\omega| \le \omega_{n+1} + \tau_{n+1} \\ \sin\{\frac{\pi}{2}\beta[\frac{1}{2\tau_n}(|\omega| - \omega_n + \tau_n)]\}, & \omega_n - \tau_n \le |\omega| \le \omega_n + \tau_n \\ 0, & otherwise \end{cases} \tag{2}$$

where $\beta(x)$ is defined as

$$\beta(x) = x^4(35 - 84x + 70x^2 - 20x^3) \tag{3}$$

The detail coefficient $w_f(k, t)$ and approximation coefficient $w_f(0, t)$ are given as the inner product of the analyzed signal with the empirical wavelet function and the scaling function,

$$\begin{aligned} w_f(n, t) &= \langle f, \psi_n \rangle = \int f(\tau)\overline{\psi_n(\tau - t)}d\tau \\ &= F^{-1}[f(\omega)\widehat{\psi}_n(\omega)] \end{aligned} \tag{4}$$

$$\begin{aligned} w_f(0, t) &= \langle f, \varphi_1 \rangle = \int f(\tau)\overline{\varphi_1(\tau - t)}d\tau \\ &= F^{-1}[f(\omega)\widehat{\varphi}_1(\omega)] \end{aligned} \tag{5}$$

where $\widehat{\psi}_n(\omega)$ and $\widehat{\varphi}_1(\omega)$ are defined by Eqs. (1) and (2), respectively, $\overline{\psi_n(t)}$ and $\overline{\varphi_1(t)}$ represent complex conjugates

of $\psi_n(t)$ and $\varphi_1(t)$, respectively. The original signal is reconstructed as follows:

$$f(t) = w_f(0,t) * \varphi_1(t) + \sum_{n=1}^{N} w_f(n,t) * \psi_n(t)$$
$$= F^{-1}[\widehat{w}_f(0,\omega)\widehat{\varphi}_1(\omega) + \sum_{n=1}^{N} \widehat{w}_f(n,\omega) * \widehat{\psi}_n(\omega)] \quad (6)$$

where symbol $*$ indicates convolution, $\widehat{w}_f(0,\omega)$ and $\widehat{w}_f(n,\omega)$ represent the Fourier transform of $w_f(0,t)$ and $w_f(n,t)$ respectively.

Following this formalism, the empirical mode f_k is represented by

$$f_0(t) = w_f(0,t) * \varphi_1(t) \quad (7)$$
$$f_k(t) = w_f(k,t) * \psi_k(t) \quad (8)$$

Therefore, through the EWT decomposition method, an original signal $y(t)$ can be expressed as

$$y(t) = \sum_{n=1}^{N} f_k(t) \quad (9)$$

The key of reasonable segmentation of Fourier spectrum is to find the segment point N. The literature [15] gives an easy way of spectrum segmentation. First, setting the number of divided bands is N. This means we need the number of boundaries is $N+1$. Because there are two fixed boundaries of 0 and π, it is necessary to determine N-1 extra boundaries. Second, the number of maxima M in Fourier spectra is calculated. Finally, compare the numerical values of N and M, if $N < M$, take the N maxima values with the highest amplitude, and then set the intermediate position of the adjacent maxima as the boundary. If $N > M$, the number of N needs to be reset, reduce the number of N to M, similarly, take the middle position of the extreme points M as the boundary. Figure 1 shows the original vibration waveform of a rolling bearing with a fault. When the number of divided bands is set to 12, the result of segmentation using the original Fourier spectral segmentation method is displayed in Figure 2. It can be known from the Figure 2 that the segmentation boundary is concentrated in the middle of the spectrum. Although the analysis accuracy of the certain frequency bands is improved by this segmentation method, it affects the analysis effect of the EWT method on other frequency ranges.

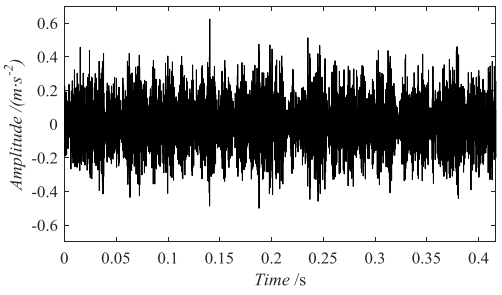

FIGURE 1. Vibration waveform of a faulty bearing.

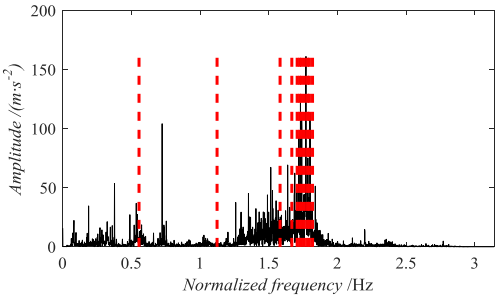

FIGURE 2. Fourier spectral segmentation of a faulty bearing vibration signal.

B. IMPROVED EMPIRICAL WAVELET TRANSFORM METHOD

The original EWT can obtain good results when analyzing signals with less frequency components and simpler spectrum. However, the rolling bearing fault contains more complicated frequency components in the above actual working environment, and the initial Fourier spectral segmentation method is no longer applicable. Therefore, this paper improves the Fourier spectral segmentation method and proposes an improved EWT (IEWT) method. The main steps of IEWT are given as follows:

(1) The spectrum of the raw signal is normalized to $[0, \pi]$, and set the number of empirical modes to be decomposed is N, find the position of all extreme points in the Fourier spectrum and count the number of maxima N_{max} and minima N_{min} respectively.

(2) If $N_{max} > 5N$, go to step (3), otherwise skip to step (4). Here, the five-fold relationship between N_{max} and N is to prevent the number of maximum values after the last processing from being smaller than the number of empirical modes N that need to be decomposed.

(3) All adjacent maxima are connected (maxima envelope), and the maximum value of the Fourier spectrum and its position are counted, the number of them is set to N_{max}, then return to step (2). Here, cubic spline interpolation is not used in the maxima envelope, because it will produce an upper or lower envelope phenomenon which causes the offset of the extreme point position, and the segmentation effect is affected.

(4) The first N maxima having the highest amplitude among the maximum value N_{max} are extracted, and the midpoint of each adjacent maximum in the N maxima is set to $L_{mid}(i), i = 1, 2, \cdots, N-1$. The position of $L_{min}(j), j = 1, 2, \cdots, N-1$ closest to the position of $L_{mid}(i)$ is taken as the Fourier spectrum division point, 0 and π are the fixed division points in the normalized Fourier spectrum. Therefore, the Fourier spectral segmentation band is defined as:

$$Bound(l) = \begin{cases} [0, L_{min}(1)], & l = 1 \\ [L_{min}(l-1), L_{min}(l)], & l = 2, 3, \cdots, N-1 \\ [L_{min}(N-1), \pi], & l = N \end{cases} \quad (10)$$

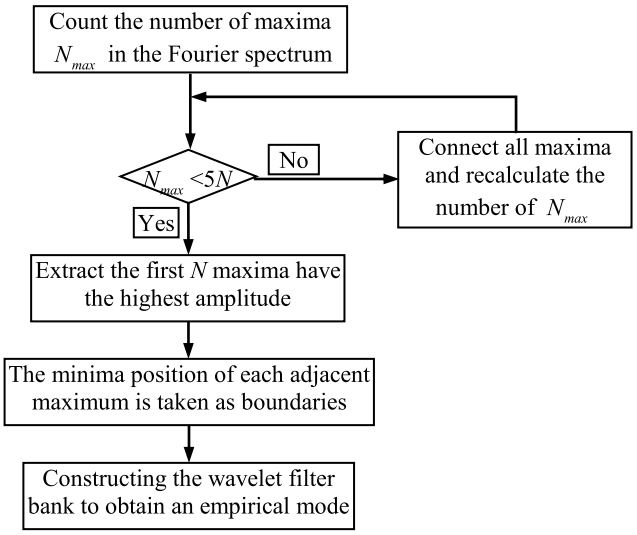

FIGURE 3. The flow diagram of IEWT.

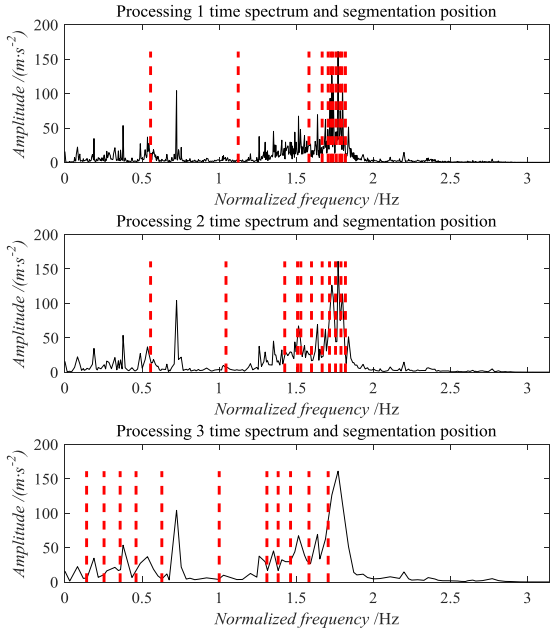

FIGURE 4. Fourier spectrum of different processing times and its division position.

Note that the minimum value of the normalized spectrum that has not been processed in the step (2) is used here because the minimum value obtained after processing is essentially the maximum value of the spectrum before processing.

The flow diagram of IEWT proposed in this paper is displayed in Figure 3.

Next, the spectrum of the above faulty bearing signal is segmented by the proposed IEWT method. The three graphs in Figure 4 are the spectral shapes connected 1∼3 times of the maximum values in the original normalized Fourier spectrum and the boundaries respectively. The number of maxima after each treatment is about 1/3 of that before processing. Therefore, the number of maxima in the original Fourier spectrum and the Fourier spectrum processed 1∼3 times

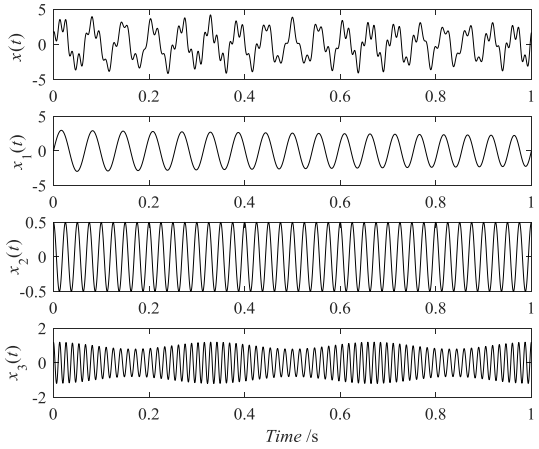

FIGURE 5. The waveform of mixed signal x(t) and its three constituent components.

are: 825, 266, 89, 26 respectively. Compared Figure 2 with Figure 4, it can be found that the Fourier spectrum is gradually smoothed with the number of times of processing, and the dominant frequency (maximum value) of each local position in the spectrum is retained. As the number of processing increases, the entire Fourier spectrum is gradually distributed by the boundary, which makes the frequency band where the dominant frequency of the local position is segmented. The segmentation method proposed in this paper lays a good foundation for subsequent signal analysis and processing.

C. SIMULATION SIGNAL ANALYSIS

To illustrate the superiority of IEWT to the existing EMD and EWT methods, first, we construct a superimposed signal $x(t)$ as Eq. (11):

$$x(t) = x_1(t) + x_2(t) + x_3(t), \quad t \in [0, 1] \tag{11}$$

where $x_1(t) = 3e^{(-0.3t)}\sin(30\pi t + 6\pi t^2)$, $x_2(t) = 0.5\cos(80\pi t)$, $x_3(t) = (1 + 0.2\cos(6\pi t))\cos(140\pi t + 2\sin(6\pi t))$, with sampling frequency $F_s = 2048$ and the waveforms of the simulated signal $x(t)$ and its three constituent components $x_1(t)$, $x_2(t)$, $x_3(t)$, are displayed in Figure 5.

First, the mixed signal constructed in Eq. (8) is decomposed using the IEWT method and the result is given in Figure 6(a). It can be observed from the Figure 6(a) that each mode is very consistent with the waveform of the original signal, and the obtained components imf_1, imf_2, and imf_3 correspond to the original three signals $x_1(t)$, $x_2(t)$ and $x_3(t)$, respectively. The IEWT decomposition method does not exhibit mode aliasing, except that there is a slight error at the endpoint of component imf_2. For comparison, the mixed signal also is decomposed using the EMD and EWT methods. The decomposition results of EMD and EWT are given in Figure 6(b-c). We can observe from the Figure 6(b) that the original signal $x_2(t)$ cannot be effectively decomposed by EMD. The obtained components imf_1, imf_2 have mode aliasing and are different from the original signals $x_3(t)$ and $x_1(t)$. From the Figure 6(c) it can be found that $x_3(t)$ can be

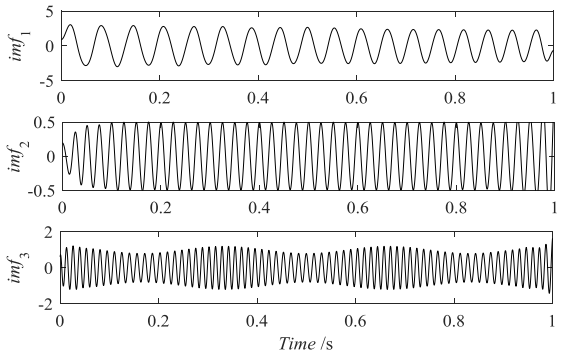

(a) The results of IEWT decomposition

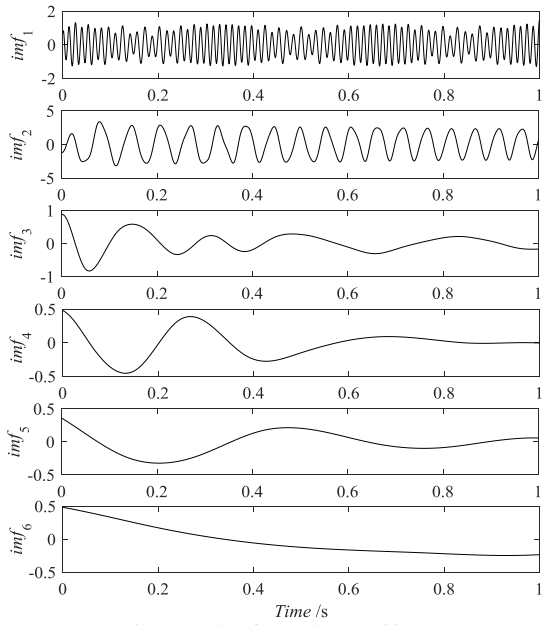

(b) The results of EMD decomposition

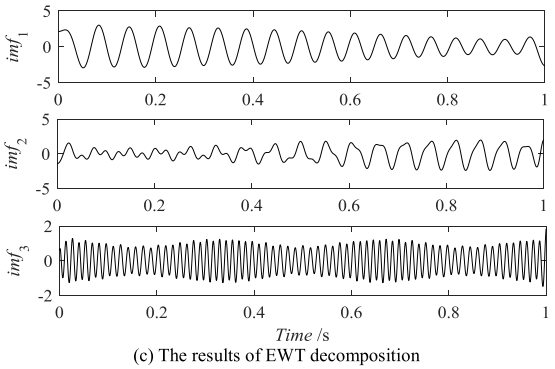

(c) The results of EWT decomposition

FIGURE 6. The results obtained by three decomposition methods of IEWT, EMD and EWT.

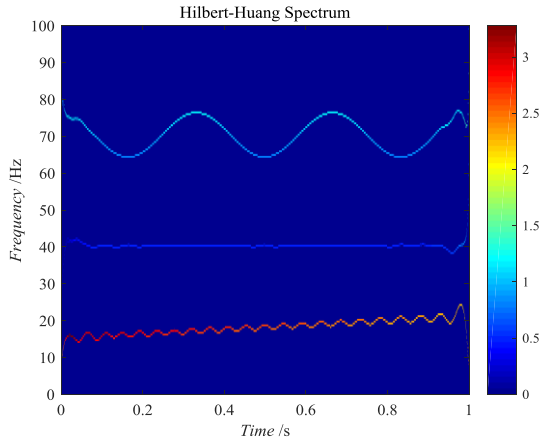

(a) The time-frequency distribution of IEWT

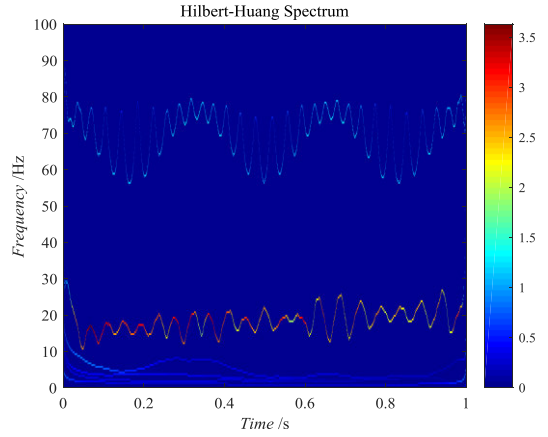

(b) The time-frequency distribution of EMD

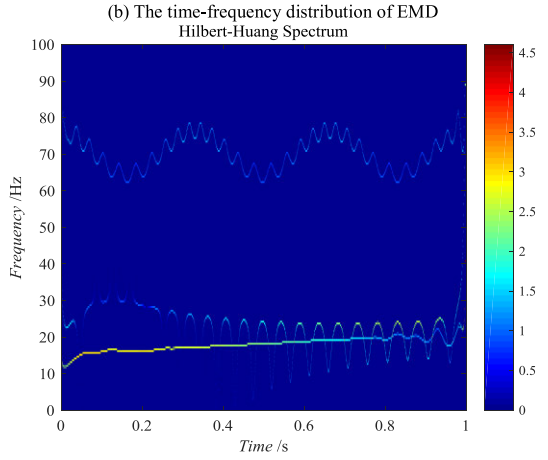

(c) The time frequency distribution of EWT

FIGURE 7. The time-frequency distribution of IEWT, EMD and EWT.

effectively separated, but the signals $x_1(t)$ and $x_2(t)$ cannot be separated by EWT. Therefore, the above analysis indicates that the decomposition result of IEWT is better than that of EWT and EMD.

The time-frequency distribution of the intrinsic components obtained by the IEWT, EMD and EWT are presented in Figure 7(a-c). It can be found from the Figure 7(a) that the Hilbert-Huang spectrum obtained by the IEWT is closest to the theoretical time-frequency distribution. From the Figure 7(b), it can be observed that the time-frequency distribution obtained by EMD fluctuates greatly and the component with a frequency of 40 Hz is not obvious. By analyzing the Figure 7(c), it can be clearly observed that the low-frequency portion of the time-frequency distribution obtained by the EWT cannot be effectively distinguished and there is a large fluctuation.

The Fourier spectrum of the mixed signal $x(t)$ is segmented by using IEWT and EWT, and the obtained boundaries are

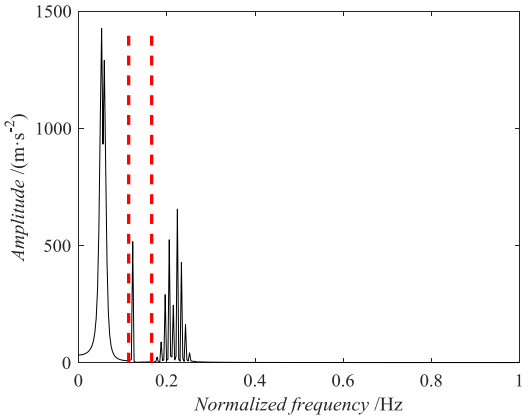

(a) The boundaries of IEWT

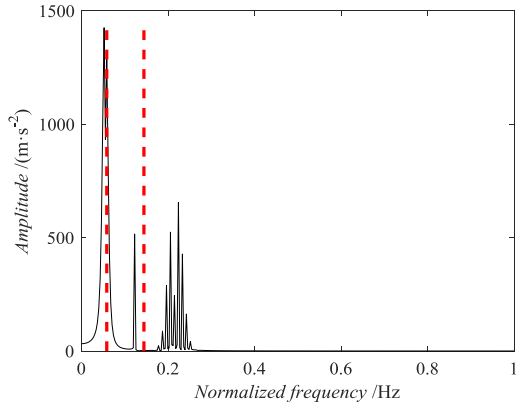

(b) The boundaries of EWT

FIGURE 8. **The spectral segmentation boundaries of IEWT and EWT.**

given in Figure 8(a-b). By analyzing Figure 8(a), it can be observed that the Fourier spectrum is effectively divided into three frequency bands, which are corresponding to the original signals of $x_1(t)$, $x_2(t)$ and $x_3(t)$. However, the first and the second bands are not effectively separated by the first boundary obtained in Figure 8(b). Simultaneously, the high frequency part of the first band is split into the second frequency band. From the decomposition result of the Figure 6(c), we can find that the second half of the first component has a lower amplitude, and the imf_2 is more complicated than the raw signal $x_2(t)$, because some information of $x_1(t)$ is included in imf_2.

III. REFINED COMPOSITE MULTISCALE DISPERSION ENTROPY METHOD

The dispersion entropy algorithm is a powerful nonlinear dynamic tool for measuring the irregularity of original vibration signals and it has the advantage of fast calculation speed and has considered the relationship between the amplitudes, but the information contained in the data cannot be fully measured by the single-scale. Therefore, multi-scale analysis based on coarse graining time series is applied to many fields and performed to extract the fault features of different scales of the signal. In this paper, RCMDE is used as a rolling bearing fault feature representation tool. The calculation process of RCMDE are shown as follows:

(1) For original signal $u(i), i = 1, 2, \cdots, L$ with a data length of L, the k-th coarse grained sequence for the scale factor of τ can be given by Eq. (12)

$$x_{k,j}^{\tau} = \frac{1}{\tau} \sum_{i=k+\tau(j-1)}^{k+j\tau-1} u_i, \quad 1 \le j \le \frac{L}{\tau}, \ 1 \le k \le \tau \tag{12}$$

(2) For each scale τ, RCMDE can be obtained from the following formula:

$$RCMDE(X, m, c, d, \tau) = -\sum_{\pi=1}^{c^m} \overline{p}(\pi_{v_0 v_1 \cdots v_{m-1}}) ln(\overline{p}(\pi_{v_0 v_1 \cdots v_{m-1}})) \tag{13}$$

where m is the embedding dimension, usually obtains a value of 2 or 3, c is the number of class, it obtains an integer between 3 and 9, the time delay d is generally taken as 1, and $\overline{p}(\pi_{v_0 v_1 \cdots v_{m-1}}) = (1/\tau) \sum_1^{\tau} p_k^{\tau}$ is the average of the dispersion pattern $\pi_{v_0 v_1 \cdots v_{m-1}}$ probabilities of the coarse-grained sequence x_k^{τ} defined in Eq. (12).

The probability $p(\pi_{v_0 v_1 \cdots v_{m-1}})$ of each dispersion pattern $\pi_{v_0 v_1 \cdots v_{m-1}}$ is:

$$p(\pi_{v_0 v_1 \cdots v_{m-1}}) = \frac{Number(\pi_{v_0 v_1 \cdots v_{m-1}})}{J - (m-1)d} \tag{14}$$

where $J = L/\tau$, the dispersion pattern $\pi_{v_0 v_1 \cdots v_{m-1}}$ consists of m numbers and each of which can be one of the integers from 1 to c.

The lost information during the coarsening process of MDE algorithm can be effectively improved by the refined composite processing method of RCMDE, which has overcome the shortcomings of the existing multi-scale entropy method. According to the paper [25], the parameters of RCMDE used in this paper are as follows: $m = 3$, $c = 6$, $d = 1$.

IV. THE ROLLING BEARING FAULT DIAGNOSIS METHOD BASED ON IEWT AND RCMDE

The flow diagram of the new diagnosis method for rolling bearing proposed in this paper is displayed in Figure 9.

The specific implementation process of the fault diagnosis method based on IEWT combining with RCMDE are listed as follows:

(1) Assume that there are K-th types rolling bearing data and $Y_1, Y_2, \cdots, Y_K$ samples are collected for each type of data. All samples of each class are decomposed using IEWT and several components are obtained for each sample.

(2) The RCMDE of each component obtained by IEWT is computed and r features from each sample can be obtained to form the feature matrix $Y_K \times r$, where $r = \lambda \times \tau_{max}$, λ is the number of IMF components obtained by IEWT decomposition, and τ_{max} is the largest scale factor in the RCMDE algorithm.

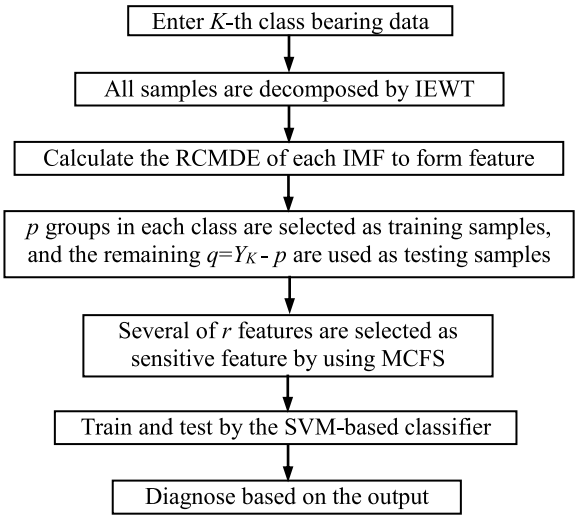

FIGURE 9. Flow diagram of the fault diagnosis method.

(3) For each class, p samples are used as training and others $q = Y_K - p$ samples are used as testing samples. Using MCFS to select the most important several feature elements that are most closely related to the fault information in the initial feature sets with dimension $Y_K \times r$. The feature order obtained by MCFS are used to select the sensitive testing samples.
(4) The sensitive features are input to the SVM for training, and the testing sample sets are tested by the trained classifier model.

V. EXPERIMENTAL DATA ANALYSIS OF ROLLING BEARING

In this subsection, the new fault diagnosis method is applied to the actual data analysis to illustrate the powerful availability of the fault method proposed in the paper. Here, rolling bearing experimental data [26] of the Case Western Reserve University (CWRU) Bearing Data Center are used, and the test stand used to collect data is presented in Figure 10. The designation of the tested bearing is 6205-2RS JEM SKF, a single point of failure on the bearing is seeded to the inner and outer race, together with the rolling element. The experimental conditions used were shown as follows: load 3 hp, motor rotation speed 1730 r/min, and frequency 12 kHz. Considering the normal signal (labeled as Norm), and rolling ball element (BE) fault, outer ring (OR) fault, inner ring (IR) fault, where BE, OR and IR are selected for two different diameters, and finally a total of 7 states are selected. Each state contains 29 samples with a length of 4096 points and thus a total of 203 samples are used. The bearing class labels 1, 2, 3, 4, 5, 6, and 7 correspond to Norm, IR1, IR2, BE1, BE2, OR1, and OR2, respectively. The fault diameter of IR1, BE1, and OR1 is 0.1778mm, and the fault diameter of IR2, BE2, and OR2 is 0.5334mm.

First, the above experimental data were analyzed by using the proposed method. 29 samples of each class are decomposed using IEWT, where in IEWT the number of IMF λ is

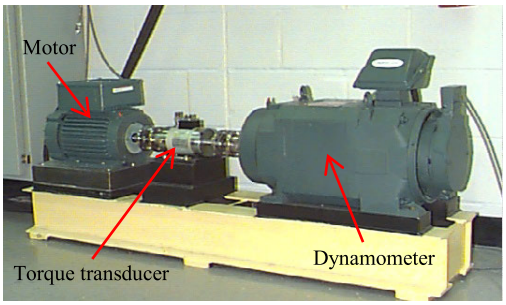

FIGURE 10. The test stand of CWRU.

set as 9 and thus for each sample nine IMF components can be obtained. Next, for each sample, the RCMDEs with scale factor $\tau_{max} = 15$ of all nine IMF components are computed. Thus, 135 ($r = \lambda \times \tau_{max} = 135$) features can be obtained for each sample. Each class of bearing data constitutes a feature set with dimension 29×135. Also, we compute the mean standard deviation of 15 scales RCMDE of each component and the results are presented in Figure 11. From the perspective of entropy deviation, the error of each type of fault is very small, which indicates that the RCMDE obtained by IEWT is very stable. From the point of view of discrimination, the result of the proposed fault diagnosis method has a relatively high degree of discrimination in most dimensions.

To verify the stability and high discrimination effect for different fault class of the proposed method, first IEWT is replaced by EMD and EWT methods to compute the RCMDE. Similarly, we can obtain the mean standard deviation of RCMDE based on EMD and EWT, where the minimum number of IMF components decomposed for each sample using EMD and EWT also is set as 9 and the detection method of EWT is 'locmax'. The mean standard deviation of RCMDE with 15 scales based on EMD and EWT of each IMF component are shown in Figure 12(a-b). From the point of view of discrimination, the RCMDE values of each fault type in the dimensions of the first two IMFs of are very close in the Figure 12(a), which makes it difficult to distinguish fault class. From the perspective of entropy deviation, it can be observed from the Figure 12(b) that the Norm, IR1 and OR2 have large errors and poor stability. From the Figure 11 and Figure 12(a-b), it can be seen that the standard deviation of RCMDE based on IEWT is smaller and the degree of discrimination is more obvious than the two comparison methods.

Second, for each class, the number of training data is 15 samples and the remaining 14 ones are selected for testing. Correspondingly, the training sample sets with dimension 15×135 are selected for each class and the other 14×135 ones are used as testing sample sets. Using MCFS to learn the training samples with the most important feature elements are selected as sensitive features. The order of selected sensitive features are used to select the sensitive testing samples. Here the first nine sensitive features selected using MCFS are selected from the 135 features to construct training data sets with dimension 15×9 and the testing ones with dimension

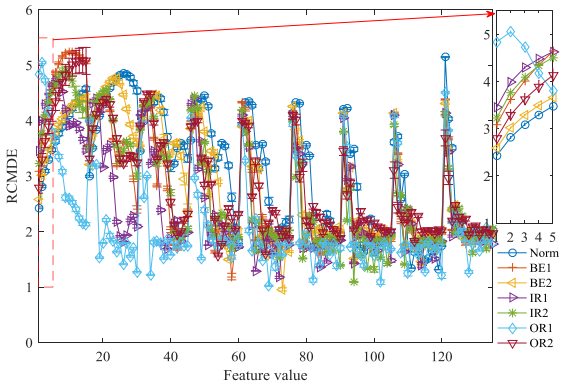

FIGURE 11. Mean standard deviation of RCMDE based on IEWT decomposition.

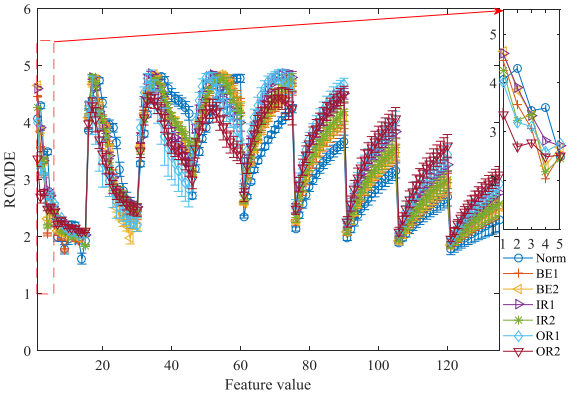

(a) Mean standard deviation of RCMDE based on EMD decomposition

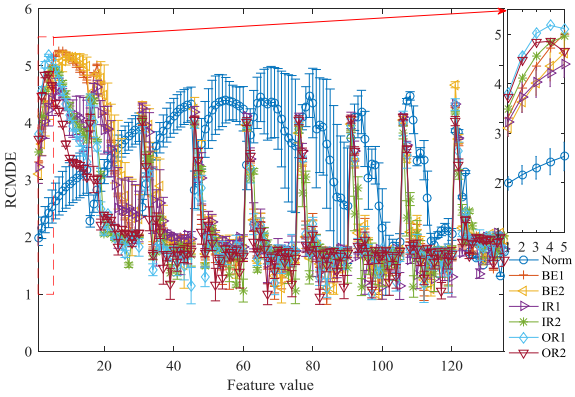

(b) Mean standard deviation of RCMDE based on EWT decomposition

FIGURE 12. Mean standard deviation of RCMDE based on EMD and EWT decomposition.

14 × 9. The SVM is used to train the sensitive features of training sample sets, where the kernel function type is set to the default value of 2, which is the radial basis function (RBF), and the value of kernel parameter used in experiment is defaults. After the testing sample sets with dimension 14×9 are predicted by using the trained classifier and the prediction results of all testing samples for the proposed diagnosis method is shown in Figure 13. It can be observed that the proposed method can effectively distinguish the 7 states of bearings and the identification rate reaches 100%, which illustrated the powerful effect of the new fault diagnosis method.

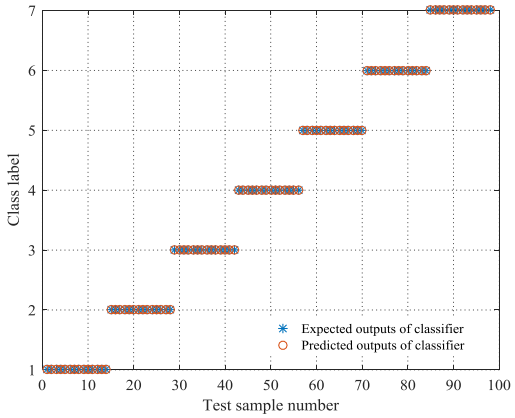

FIGURE 13. The prediction results of RCMDE combining with IEWT.

TABLE 1. Comparison of identifying rate of the three methods.

Methods	misclassified sample	Identifying rate
EMD-RCMDE - MCFS-SVM	4	95.92%
EWT-RCMDE - MCFS-SVM	6	93.88%
IEWT-RCMDE - MCFS-SVM	0	100%

For comparison purpose, the IEWT used in the new method of rolling bearing fault diagnosis was replaced by EMD and EWT and the parameter of EMD and EWT are set as described above. Similar to the proposed diagnosis method, next, for the initial fault features obtained by EMD and EWT methods, sensitive features are selected by MCFS. Then the selected fault sets are input to the SVM for training and testing. For the EMD and EWT methods, the prediction results are presented in Figure 14(a-b) respectively, and the obtained identifying rates results are summarized in Table 1. It can be found from the Figure 14(a) that there are 4 samples of the 98 testing ones are misclassified by the RCMDE and EMD method and the result of identification rate is 95.92%. In Figure 14(b) there are 6 samples are incorrectly assigned to other fault types by the RCMDE and EWT-based method and the identification rate is 93.88%. The obtained identification rates indicate that the IMF components decomposed by IEWT are more conducive to fault identification than that of EMD and EWT methods and the superiority of the proposed new method also been demonstrated.

Next, to verify the effectiveness and superiority of RCMDE in multiscale feature extraction, RCMDE is replaced by DE and MDE with combing with MCFS and SVM in the proposed method. That is, when using the IEWT method to decompose all samples, the DE and MDE with 15 scales are computed of all IMFs. The mean standard deviation of DEs for all IMFs obtained using IEWT is shown in Figure 15, from which it can be found that this method has a relatively large error in the latter three components of the OR2, the standard deviation of other bearing data is very small. Meanwhile,

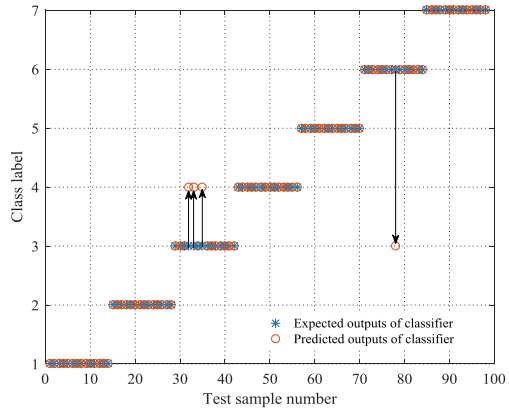

(a) The prediction results of RCMDE combining with EMD

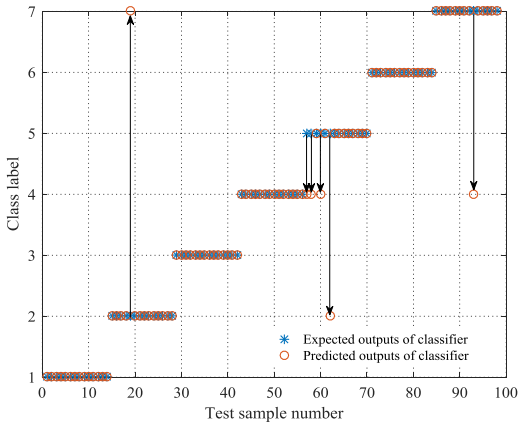

(b) The prediction results of RCMDE combining with EWT

FIGURE 14. The prediction results of RCMDE combining with IEWT, EMD and EWT.

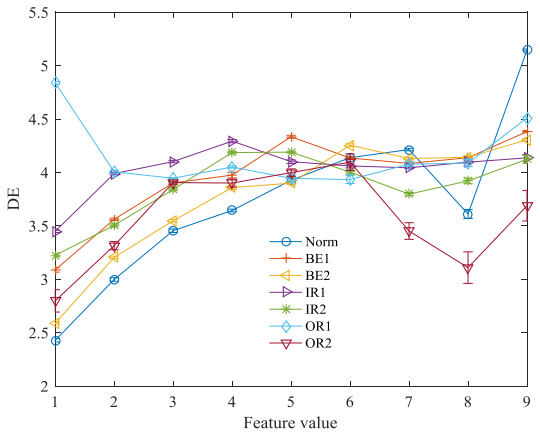

FIGURE 15. Mean standard deviation of DE based on IEWT.

number of DEs are overlapped. Similarly, the mean standard deviation of MDE based on IEWT are also computed and shown in Figure 16, from Figure 11 and Figure 16 it can be found that the results of MDE and RCMDE are very consistent, but the standard deviations of MDE are greater than that of RCMDE in some dimensions, which indicates that RCMDE is more stable than MDE and the advantage of RCMDE is verified.

Further, to demonstrate the necessity of MCFS in the new diagnostic method, the original vibration signals are

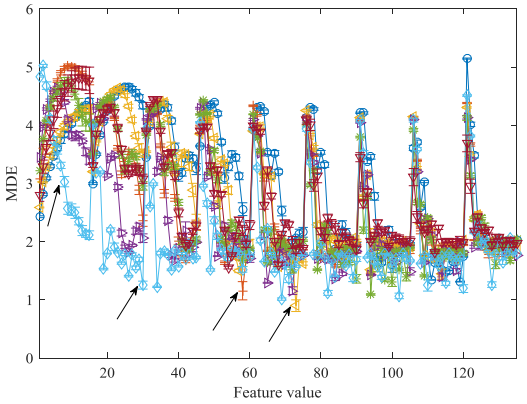

FIGURE 16. Mean standard deviation of MDE based on IEWT.

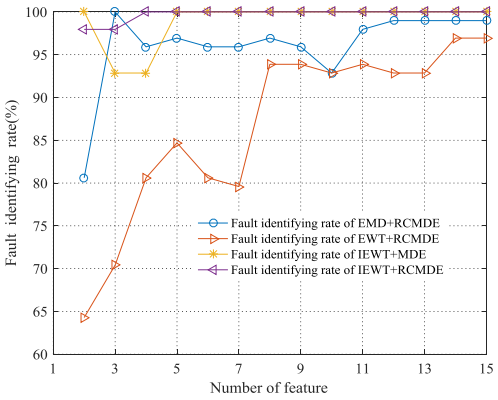

FIGURE 17. Identification rates of different feature numbers for the four methods.

TABLE 2. Comparison of identifying rate of the three methods without using MCFS.

Methods	misclassified sample	Identifying rate
EMD-RCMDE - SVM	5	94.90%
EWT-RCMDE - SVM	3	96.94%
IEWT-RCMDE - SVM	1	98.98%

decomposed by IEWT, EMD and EWT respectively. Without loss of generality, the RCMDE of the first two IMF components are computed, i.e. 30 values obtained are directly used as the sensitive faults and input to the SVM for training and testing with the same training and testing data as the proposed method. The identifying rates of RCMDE based on IEWT, EMD and EWT are shown in Table 2. Through the comparison of Table 1 and Table 2, it can be found that the identifying rates of RCMDE based on EMD and IEWT without using MCFS are lower than those methods by using MCFS. The necessity of MCFS for feature selection was verified by the comparison results of identifying rates.

Finally, the effect of different number of sensitive fault features on the identification rate is studied. For the proposed

TABLE 3. The features selected by MCFS in the IEWT+RCMDE method.

No. of feature	Selected feature dimension	No. of feature	Selected feature dimension
2	94,14	9	120,79,49,52,91,1,64, 58,96
3	120,58,14	10	120,79,49,52,91,64,1,19,56,106
4	120,58,14,79	11	120,49,79,64,1,91,52,19,56,106,73
5	120,58,91,64,79	12	120,49,79,64,1,91,52,19,106,56,73,53
6	120,41,91,79,49,13	13	120,49,79,1,64,52,91,106,19,56,73,53,14
7	120,41,79,91,49,64,1	14	120,49,1,64,52,79,91,106,19,56,73,53,14,25
8	120,79,49,41,91,64,1,58	15	120,1,49,64,52,91,79,106,56,73,19,53,14,25,75

TABLE 4. The features selected by MCFS in the IEWT+MDE method.

No. of feature	Selected feature dimension	No. of feature	Selected feature dimension
2	120,94	9	91,49,56,13,120,75,107,88,79
3	120,65,91	10	91,49,75,120,56,13,79,107,8,42
4	120,73,88,38	11	91,49,75,120,56,79,13,107,8,106,41
5	120,13,91,88,49	12	49,75,120,79,91,13,107,56,8,106,77,64
6	120,13,91,49,88,107	13	49,120,13,107,91,75,106,8,77,79,64,41,56
7	91,13,49,56,42,120,88	14	120,49,107,91,13,75,77,106,8,64,79,38,41,55
8	91,13,49,56,75,88,120,8	15	120,107,49,91,8,13,77,106,75,64,38,79,41,55,54

TABLE 5. The features selected by MCFS in the EMD+RCMDE method.

No. of feature	Selected feature dimension	No. of feature	Selected feature dimension
2	4,2	9	9,15,24, 1,75,26, 4,17,56
3	4,45,24	10	9,15,75,24, 1,17,23,56,20,14
4	24, 4,56, 1	11	15, 9, 1,24,75, 3,20,23, 2,28, 4
5	24,56, 4, 9, 1	12	15, 9, 1,24, 3,75,20,23, 8, 4,28, 2
6	9,24, 4,56, 1,17	13	15, 9, 1, 3,20,23, 8,24,75, 4, 5,56,34
7	9,24, 1, 4,15,17,75	14	15, 1, 8,20, 3,19, 9,23, 5, 4,75,31,56,24
8	9,24,15, 1,17, 4,75,26	15	15, 8,20, 1, 3,19,23, 9, 5, 4,56,75,31,36,54

TABLE 6. The features selected by MCFS in the EWT+RCMDE method.

No. of feature	Selected feature dimension	No. of feature	Selected feature dimension
2	47,119	9	28,15,43,30,64,115,74,47,20
3	69,86,20	10	28,15,30,43,115,74,47,64,33,92
4	20,69,28,78	11	28,15,30,115,64,43,47,74,33,31,52
5	20,28,107,47,15	12	28,15,33,115,64,47,43,30,96,31,74,78
6	28,20,15,107,47,43	13	28,15,33,64,47,115,31,94,43,74,30,78,32
7	28,20,15,43,107,5,115	14	28,15,64,33,114,115,47,94,31,74,30,78,32,2
8	15,28,43, 5,30,20,115,17	15	28,15,64,115,114,33,94,47,74,31,38,78,32,2,100

method, the sensitive fault features with element numbers ranging from 2 to 15 are selected for training and testing by using MCFS. When 2 to 15 features are selected, the corresponding identification rate of the IEWT (or EMD, EWT) and RCMDE based fault diagnosis methods, together with IEWT and MDE based method are shown in Figure 17,

where the selected features by MCFS for the four methods are shown in Tables. 3 to 6. It can be seen that the identification rate of the new diagnosis method is higher than the other three methods. The identification rate of the proposed method in this paper reaches 100% when the number of selected sensitive features more than 3 and which is higher than the identification rate of IEWT and MDE based method when the number of selected features is 3 and 4. The other two methods require more features to achieve a better identification. Therefore, generally, we set the number of selected sensitive feature more than 5. The above analysis shows that the superiority of the new diagnosis method in actual bearing data compared with the other three methods.

VI. CONCLUSION

The proposed IEWT method differs from EWT in that it is based on the maxima envelope to overcome the limitations of original EWT. Simultaneously, the analysis result indicates that IEWT method is more reasonable for Fourier spectral segmentation than the original EWT. The advantages of IEWT to EWT and EMD is explained by the simulation and actual data analysis. On this basis, a new fault diagnosis method based on IEWT, RCMDE, MCFS and SVM for rolling bearing is proposed in this paper and applied to experimental analysis of rolling bearing. Also IEWT is compared with EMD and EWT by diagnosing experiment data and the results indicate that the proposed method has a better identification rate than EMD and EWT based ones. Besides, the advantages of RCMDE relative to DE and MDE is studied and the results show that RCMDE is outperform to DE and MDE in extracting the fault information and is more stable than MDE. Finally, we also investigated the necessity of MCFS for feature selection, together with the influence of set different sensitive fault features. In summary, the proposed new fault diagnosis method is more conducive to fault identification than the other methods of comparison. However, there are still some problems that need to be discussed, such as how to adaptively set the number of IEWT and we will study it in the future work.

REFERENCES

[1] M. Rostaghi and H. Azami, "Dispersion entropy: A measure for time-series analysis," *IEEE Signal Process. Lett.*, vol. 23, no. 5, pp. 610–614, May 2016.

[2] C. Li, J. Zheng, H. Pan, J. Tong, and Y. Zhang, "Refined composite multivariate multiscale dispersion entropy and its application to fault diagnosis of rolling bearing," *IEEE Access*, vol. 7, pp. 47663–47673, Mar. 2019.

[3] H. Azami, M. Rostaghi, D. Abasolo, and J. Escudero, "Refined composite multiscale dispersion entropy and its application to biomedical signals," 2016, *arXiv:1606.01379*. [Online]. Available: https://arxiv.org/abs/1606.01379

[4] H. Azami, M. Rostaghi, D. Abásolo, and J. Escudero, "Refined composite multiscale dispersion entropy and its application to biomedical signals," *IEEE Trans. Biomed. Eng.*, vol. 64, no. 12, pp. 2872–2879, Dec. 2017.

[5] Y. Wu and R. Song, "Stroke-related difference in electromyographic signals using refined composite multiscale dispersion entropy—A case study," in *Proc. 3rd Int. Conf. Adv. Robot. Mechtron. (ICARM)*, Singapore, Jul. 2018, pp. 685–690.

[6] N. K. Al-Qazzaz, S. H. M. Ali, and S. A. Ahmad, "Differential evolution based channel selection algorithm on eeg signal for early detection of vascular dementia among stroke survivors," in *Proc. IEEE-EMBS Conf. Biomed. Eng. Sci. (IECBES)*, Sarawak, Malaysia, Dec. 2018, pp. 239–244.

[7] N. E. Huang, Z. Shen, S. R. Long, M. C. Wu, H. H. Shih, Q. Zheng, N.-C. Yen, C. C. Tung, and H. H. Liu, "The empirical mode decomposition and the Hilbert spectrum for nonlinear and non-stationary time series analysis," *Proc. Roy. Soc. London A, Math., Phys. Eng. Sci.*, vol. 454, no. 1971, pp. 903–995, Mar. 1998.

[8] J. B. Ali, N. Fnaiech, L. Saidi, B. Chebel-Morello, and F. Fnaiech, "Application of empirical mode decomposition and artificial neural network for automatic bearing fault diagnosis based on vibration signals," *Appl. Acoust.*, vol. 89, no. 3, pp. 16–27 Mar. 2015.

[9] J. Han and M. van der Baan, "Empirical mode decomposition for seismic time-frequency analysis," *Geophysics*, vol. 78, no. 2, pp. 9–19, Feb. 2013.

[10] S. Pal and M. Mitra, "Empirical mode decomposition based ECG enhancement and QRS detection," *Comput. Biol. Med.*, vol. 42, pp. 83–92, Jan. 2012.

[11] Y. Lei, J. Lin, Z. He, and M. J. Zuo, "A review on empirical mode decomposition in fault diagnosis of rotating machinery," *Mech. Syst. Signal Process.*, vol. 35, nos. 1–2, pp. 108–126, Feb. 2013.

[12] Z. X. Li *et al.*, "Decoupling of multiple concurrent faults for diagnosing coal-cutter gearboxes: An extensive experimental investigation with multichannel sensor measurements," *ASME J. Nondestruct. Eval., Diagnostics Prognostics Eng. Syst.*, vol. 2, pp. 1–49, Aug. 2019.

[13] Z. Li, Y. Jiang, Z. H. Duan, and Z. Peng, "A new swarm intelligence optimized multiclass multi-kernel relevant vector machine: An experimental analysis in failure diagnostics of diesel engines," *Struct. Health Monit.*, vol. 17, no. 6, pp. 1503–1519, Jan. 2018.

[14] Y. Lei, Z. He, and Y. Zi, "Application of the EEMD method to rotor fault diagnosis of rotating machinery," *Mech. Syst. Signal Process.*, vol. 23, no. 4, pp. 1327–1338, May 2009.

[15] J. Gilles, "Empirical wavelet transform," *IEEE Trans. Signal Process.*, vol. 61, no. 16, pp. 3999–4010, Aug. 2013.

[16] Z. Li, T. Yu, and D. Wu, "Prediction of material removal rate for chemical mechanical planarization using decision tree-based ensemble learning," *ASME J. Manuf. Sci. Eng.*, vol. 141, no. 3, Aug. 2019, Art. no. 031003.

[17] A. Bhattacharyya and R. B. Pachori, "A multivariate approach for patient-specific EEG seizure detection using empirical wavelet transform," *IEEE Trans. Biomed. Eng.*, vol. 64, no. 9, pp. 2003–2015, Sep. 2017.

[18] S. Maheshwari, R. B. Pachori, and U. R. Acharya, "Automated diagnosis of glaucoma using empirical wavelet transform and correntropy features extracted from fundus images," *IEEE J. Biomed. Health Inform.*, vol. 21, no. 3, pp. 803–813, May 2017.

[19] W. Liu, S. Cao, and Y. Chen, "Seismic time-frequency analysis via empirical wavelet transform," *IEEE Geosci. Remote Sens. Lett.*, vol. 13, no. 1, pp. 28–32, Jan. 2016.

[20] B. Merainani, C. Rahmoune, D. Benazzouz, and B. Ould-Bouamama, "Rolling bearing fault diagnosis based empirical wavelet transform using vibration signal," in *Proc. Int. Conf. Modeling Identificat. Control (ICMIC)*, Algiers, Algeria, Nov. 2016, pp. 526–531.

[21] S. N. Chegini, A. Bagheri, and F. Najafi, "Application of a new EWT-based denoising technique in bearing fault diagnosis," *Measurement*, vol. 144, pp. 257–297, Oct. 2019.

[22] W. Deng, S. Zhang, H. Zhao, and X. Yang, "A novel fault diagnosis method based on integrating empirical wavelet transform and fuzzy entropy for motor bearing," *IEEE Access*, vol. 6, pp. 35042–35056, May 2018.

[23] D. Cai, C. Zhang, and X. He, "Unsupervised feature selection for multi-cluster data," in *Proc. 16th ACM SIGKDD Int. Conf. Knowl. Discovery Data Mining (KDD)*, New York, NY, USA, Jul. 2010, pp. 333–342.

[24] C.-C. Chang and C.-J. Lin, "LIBSVM: A library for support vector machines," *ACM Trans. Intell. Syst. Technol.*, vol. 2, no. 27, Jun. 2007, Art. no. 27.

[25] M. M. Rahman, M. I. H. Bhuiyan, and A. R. Hassan, "Sleep stage classification using single-channel EOG," *Comput. Biol. Med.*, vol. 102, pp. 211–220, Nov. 2018.

[26] J. Zheng, H. Pan, S. Yang, and J. Cheng, "Generalized composite multiscale permutation entropy and Laplacian score based rolling bearing fault diagnosis," *Mech. Syst. Signal Process.*, vol. 99, pp. 229–243, Jan. 2018.